MODELS FOR MEASURING EXPLOSION ENERGIES AND ISM DENSITIES OF SUPERNOVA REMNANTS IN THE GALAXY

D. A. LEAHY

Dept. Physics and Astronomy, University of Calgary, Calgary, Alberta, Canada T2N 1N4
E–mail: leahy@ucalgary.ca

Abstract. Supernova remnant (SNR) models have been developed to explain the observed characteristics of SNRs, and thus to deduce their physical properties. One important part of modelling is use of hot plasma (X-ray) emission models to derive temperature and amount of shocked plasma and the SNR shock velocity. Coupled with a SNR evolution model, one can use the current state of a SNR to deduce fundamental properties of the supernova (SN) explosion. The general phases of SNR evolution are the ejecta-dominated phase, the adiabatic phase and the radiative phase. The transition phases between these are less-appreciated but at least as important, because the transition phases account for much of the total lifetime of a SNR. Progress in X-ray observations of SNRs has resulted in a significant sample of Galactic SNRs with measured X-ray spectra. We have developed spherically symmetric models over the past few years (Leahy and Williams 2017, Leahy et al. 2019) which allow inference of SNR explosion energy, circumstellar medium density and age. With detailed enough X-ray spectra, ejecta mass and whether the SN occurs in a uniform or stellar wind environment can also be determined. We have applied the models to observations of LMC SNRs (Leahy 2017) and of Galactic SNRs (Leahy and Ranasinghe 2018, Leahy et al. 2020). We find that the energy and density distributions can be well fit with log-normal distributions and that SNR birth-rates are consistent with SN rates.

1. INTRODUCTION

Various areas in astrophysics are impacted by the energy and mass input to the interstellar medium in galaxies by supernovae (SN) and their remnants (SNR). These areas include stellar evolution, the physical and chemical evolution of the interstellar medium (ISM, e.g. see Cox 2005 for a review) and the subsequent impact on star formation and evolution of galaxies. Studying SNRs is one of the best ways of measuring the kinetic energy input of SN into the ISM (Cox 2005).

SNRs are observed in radio, infrared, optical, X-ray and gamma-ray bands (see, e.g. Bandiera 2001 for a review). The radio emission is a tracer of relativistic electrons accelerated by the SNR shock, with these electrons containing <1% of the SN energy. The infrared emission is from shock heated dust and the optical line emission from small clouds of dense gas recombining behind the shock. The X-rays are from the plasma heated by the SNR shock, with temperature ∼1 keV and are a measure of the bulk energy of the SN explosion as most of the energy goes into shock heating of the gas. Gamma-rays are also from high energy particles, electrons and protons,

accelerated by the shock. The physics of X-ray emission is much better understood for SNRs than that of radio emission or gamma-ray emission. Infrared and optical emission are mostly sensitive to the amount of dust present and the properties of small dense clouds, respectively. Thus modelling X-ray emission, which depends mainly on the shock energy deposited in the hot gas, is most effective for determining SNR energies.

Historically, the observations of SNRs were made in radio and optical much before X-ray, infrared or gamma-ray observations. ∼300 SNRs have been observed in radio, with significantly fewer observed in other bands, including X-rays. Thus, only a small fraction of the SNRs in our Galaxy have previously been characterized well enough to determine their evolutionary state, including explosion type, explosion energy, and age. A number (∼10) historical SNRs have been observed in great detail and modeled with hydrodynamic simulations. E.g., Tycho has been modeled (Badenes et al. 2006) and used to test different models for SN Type Ia explosions.

However, most SNRs do not have comprehensive multi-band observations (imaging and spectra), so they not been the subject to detailed hydrodynamic modeling. Thus, the author has led a project to create an intermediate modelling approach (Leahy & Williams 2017, Leahy et al. 2019, Leahy et al. 2020). It is based on hydrodynamic simulations, but uses analytic and numerical fits (which we call semi-analytical) to create models which can be easily calculated and applied to SNRs. The goal is to apply this model to observationally less-constrained SNRs, to determine their bulk physical characteristics. When more detailed observations become available for any given SNR, full hydrodynamic modelling can be carried out to improve upon the results from the semi-analytical model.

Below, the basics of the SNR model are described in the Model section. The multiple stages of the model and the hydrodynamic simulations used to build the model are described. Application of the model to observations of SNRs are given in the Results section. The conclusions for explosions energies of SNRs and ISM densities are given in the Summary and Conclusions section.

2. MODEL OF SNR EVOLUTION

The basis of the model is to calculate quantities related to the observations that determine the evolutionary state of the SNR. We make the assumption of spherically symmetric evolution. The evolutionary state is determined by the initial conditions of the SNR and its age.

The main initial conditions are SN explosion energy (E_0), mass of ejected stellar envelope (M_{ej}), and circumstellar medium density (CSM) or ISM (n_0 or stellar wind parameter q). Secondary initial conditions which are next most important are: the density distribution of the stellar ejected envelope, the density distribution of the CSM or ISM. Tertiary initial conditions which also affect the evolution, e.g. for the strength of the line emission from the shocked gas and for equation of state of the plasma, are composition of the ejecta, composition of the CSM/ISM, the rate at which shocked ions and electrons come into equipartition, the CSM/ISM temperature and emissivity, and CSM/ISM turbulence velocity. The large number of input parameters makes construction of a universal model difficult. However many can be implemented by use of analytic approximations into the SNR model code.
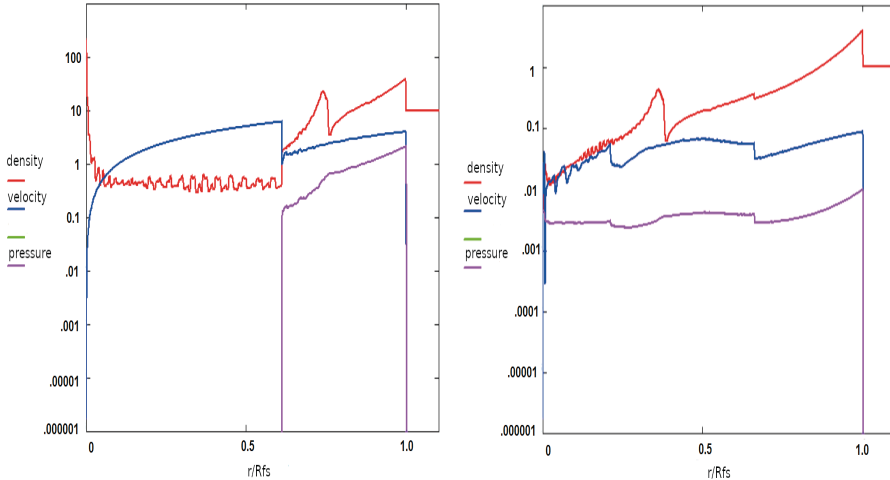
Figure 1: The interior structure of a supernova remnant for $s = 0$, $n = 8$ from hydrodynamic simulations at the characteristic times: $t/t_{\mathrm{ch}} \simeq 1$ with $R_{\mathrm{FS}}/R_{\mathrm{ch}} \simeq 1.1$ (left), and $t/t_{\mathrm{ch}} \simeq 10$ with $R_{\mathrm{FS}}/R_{\mathrm{ch}} \simeq 2.9$ (right). The density, velocity and pressure are scaled to their characteristic values, and are plotted vs. radius in units of the forward shock radius (r/R_{FS}). The vertical axis is on log scale.

To be useful in deriving the main initial conditions (E_0, M_{ej}, n_0 or q) and SNR age from observations, the model has to be able to predict the current observables of an SNR. These are (Leahy et al. 2019): the observed radius (R_{fs}) of the forward shock (fs), the X-ray emission measure (EM_{fs}) of the (fs), and the emission-measure-weighted shock temperature (T_{fs}). In cases, in particular for young SNR, where both forward and reverse shock are observed, more information can be derived on initial and secondary initial conditions.

The early evolution, prior to radiative losses, follows a unified evolution. This is described in Truelove & McKee (1999) (hereafter TM99), where the evolution of forward and reverse shock radius and shock velocity vs. characteristic (dimension-less) time are calculated. Our models (Leahy & Williams 2017, Leahy et al. 2019, Leahy et al. 2020) all include the basic TM99 model but add calculation of EM and EM-weighted temperature of the shocked gas. Leahy & Williams (2017) calculated forward-shock (fs) emission measures (EM_{fs}) and temperatures (T_{fs}) for the adiabatic phase; and calculated EM_{fs}, T_{fs}, EM_{rs} and T_{rs} and for the early self-similar ejecta dominated (ED) phase.

Leahy et al. (2019) carried out more extensive and accurate hydrodynamic simulations than previous work. Here we show of the interior structure of the SNR in Figures 1 and 2. The emphasis here is on the late time evolution, so here we show the extension of the numerical calculations to later times, up to $t/t_{\mathrm{ch}} > 1000$. A new result found is that the reverse shock propagating through the ejecta leaves behind a peak in the density profile, where the reverse shock transitions from the ejecta envelope into the ejecta core. The peak, in contrast to expectations, expands more slowly
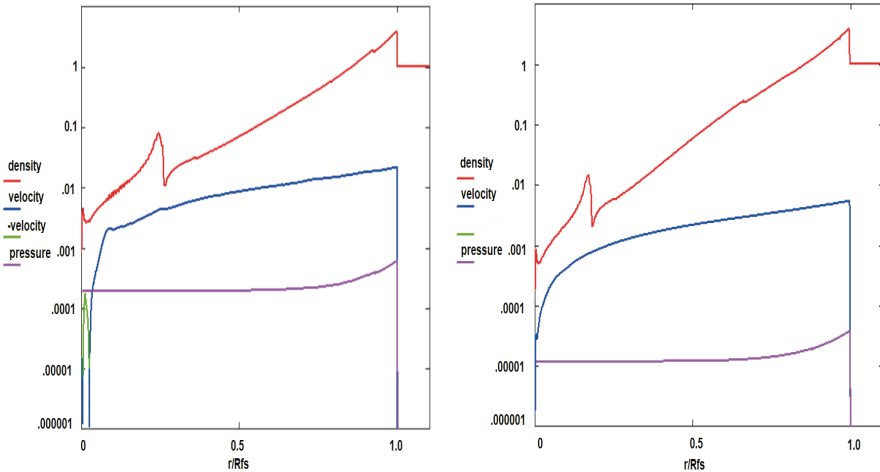
Figure 2: The interior structure of a supernova remnant for $s = 0$, $n = 8$ from hydrodynamic simulations at the characteristic times: $t/t_{\text{ch}} \simeq 100$ with $R_{\text{FS}}/R_{\text{ch}} \simeq$ 7.4 (left), and $t/t_{\text{ch}} \simeq 1000$ with $R_{\text{FS}}/R_{\text{ch}} \simeq 19$ (right). The density, velocity and pressure are scaled to their characteristic values, and are plotted vs. radius in units of the forward shock radius (r/R_{FS}). The vertical axis is on log scale.

than the simple prediction of homologous interior expansion. I.e. the radius of the shocked ejecta density peak, in units of the shock radius, decreases with time.

EM_{fs}, T_{fs}, EM_{rs} and T_{rs} were calculated by Leahy et al. (2019) directly from the hydrodynamic simulations for all SNR non-radiative stages (ED, transition ED to adiabatic, and adiabatic). E.g. Figures 6, 7 and 8 of Leahy et al. (2019) show the interior structure for the ED phase for several ejecta profiles (n= 6, 8, 10, and 12) and for constant density CSM ($s = 0$) and stellar wind profile CSM ($s = 2$). The dimensionless emission measures vs. impact parameter were shown for the above cases plus $n = 7$ and 14 in Figures 9 and 10 of Leahy et al. (2019). The complete time evolution of integrate emission measure and emission-measure-weighted temperature for both forward and reverse shocks were calculated for $s = 0$ and $s = 2$; and for each value of s all n values from 6 through 14 were calculated.

All of these results have been incorporated into the most recent release of the Python SNR modelling program SNRPy, publically available at http:\\quarknova.ca. The models include electron heating by collisions with ions, which uses the formalism of Raymond, Cox and Smith (1976).

Figures 3 and 4 here show the main panel of SNRPy, when the selected plot is radius or velocity of fs and rs vs. time. The large number of inputs available are seen on the left hand side of the graphical interface of SNRPy. Typically the rs speeds up when it enters the ejecta core, after propagating through the power-law envelope in a nearly self-similar matter. Figures 5 and 6 show EM and EM-weighted temperature of fs gas and rs gas vs. time. EM_{rs} decreases after the rs reaches the ejecta core, whereas EM_{fs} continues to increase until the SNR becomes radiative.
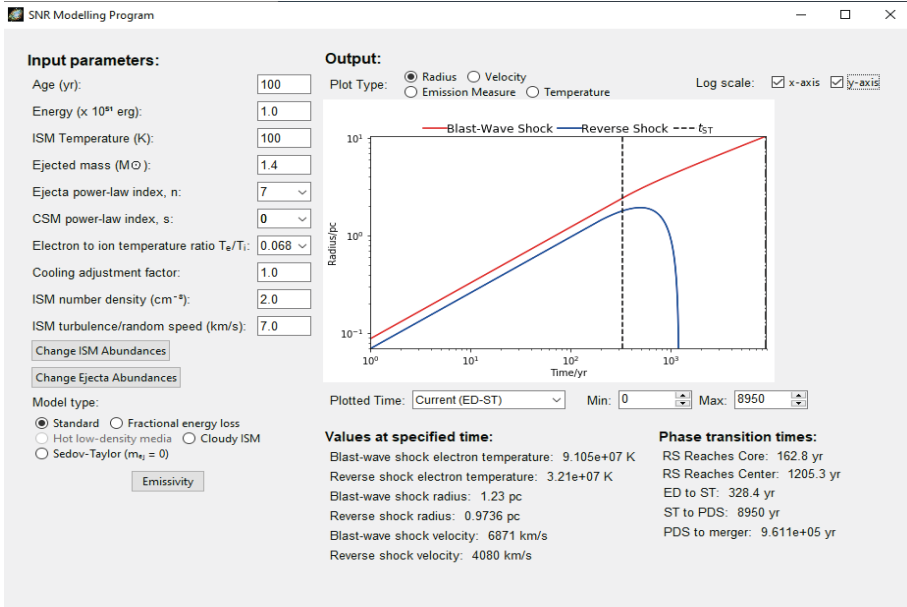
Figure 3: Screenshot of graphics interface of the SNRPy software illustrating evolution of forward and reverse shock radius vs. time. The input parameters to the model are in the left 1/3 of the panel. Output parameters are below the graph of radius vs. time.
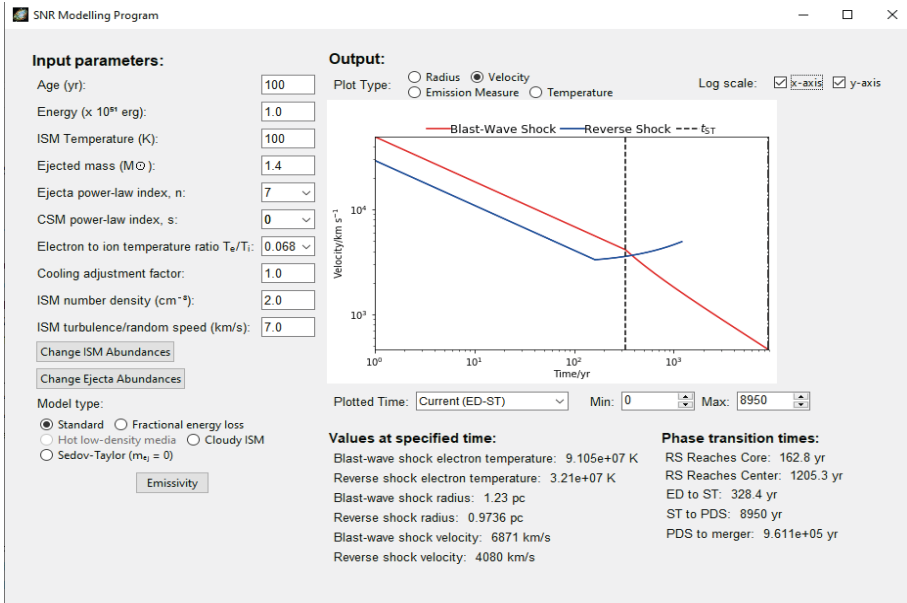

Figure 4: Screenshot of graphics interface of the SNRPy software illustrating evolution of forward and reverse shock velocity vs. time.
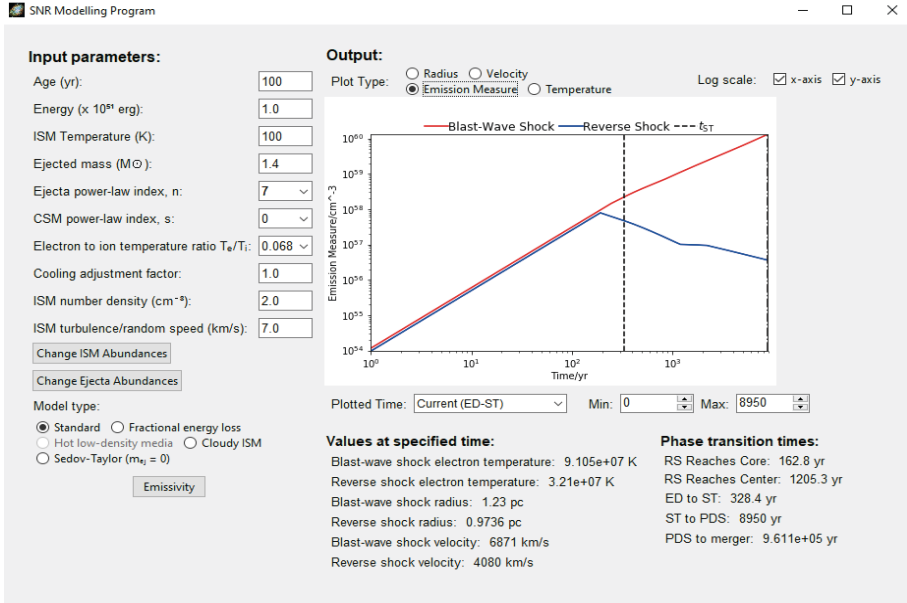
Figure 5: Screenshot of graphics interface of the SNRPy software illustrating evolution of forward and reverse shock emission measure vs. time.
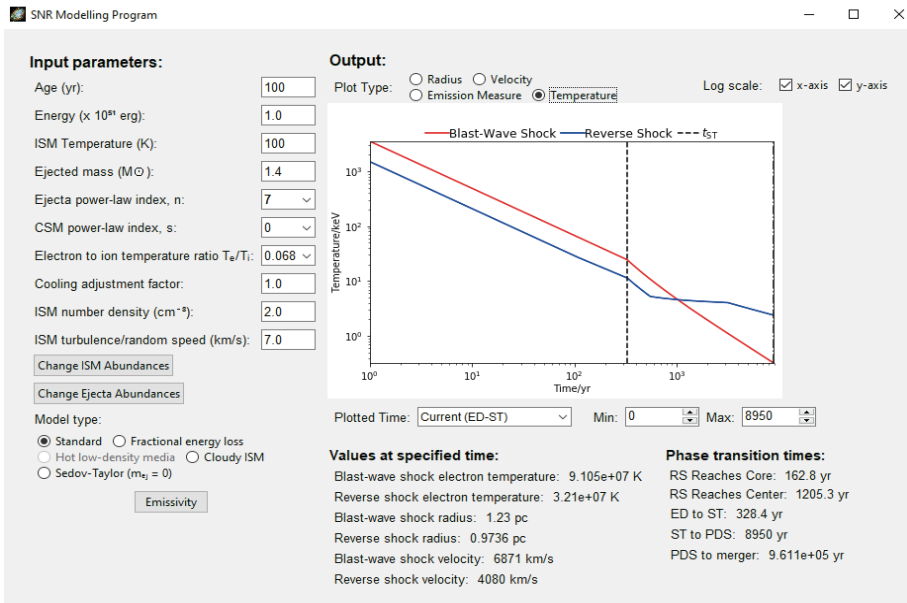

Figure 6: Screenshot of graphics interface of the SNRPy software illustrating evolution of forward and reverse shock emission-measure-weighted temperature vs. time.

3. RESULTS AND DISCUSSION

The SNR evolution model was first applied to 50 LMC SNRs with measured R_{fs}, EM_{fs}, T_{fs} (Maggi et al. 2016) by Leahy (2017). The main results were that the distribution of explosion energies (E_0) and of ISM densities (n_0) were both log-normal. A log-normal distribution is expected when a number of processes with random variables, even if each process is non-Gaussian, act in a multiplicative manner, so is not surprising in retrospect. Both the density of the ISM and the explosion process for SN are complex and involve many physical factors, with each factor have variation from location to location in the ISM, or from one SN progenitor to another. Previously it was only known that E_0 and n_0 varied from SNR to SNR. The large range of variation (about 2 orders of magnitude), the means and the shapes of the distributions for E_0, n_0) were previously unknown. The mean explosion energy was found to be 5×10^{50} erg, significantly less than the canonical explosion energy of 1×10^{51} erg, used in most simple models. This work also found the SNR birthrate for the LMC to be 1/ 500 yr, which is one of the best determinations so far.

A sample of Galactic SNRs was modelled, for the first time using emission measures and temperatures, by Leahy & Ranasinghe (2018). This work confirmed the log-normal distributions of E_0 and n_0, and that it also applied to Galactic SNRs. The mean energy and mean density for the 15 SNRs were found to be 5×10^{50} erg and 0.26 cm^{-3}, respectively. This confirmed the low mean energy of observed SNRs compared to what is usually assumed in SNR models. Table 2 of that paper also demonstrated the importance of including electron heating by ions for all derived parameters (age, E_0, and n_0).

Leahy et al. (2020) added a calculation of the inverse model, which enabled applying the rather complex model to a large number of SNRs. 43 Galactic SNRs were modelled. The sample included all SNRs, except for the historical SNRs, that had observations of the forward shock R, EM and T. These models assumed $s = 0$ and $n = 7$, in order to have the same number of output parameters (age, E_0, n_0) as input parameters. For the 7 known mixed morphology SNRs, the Cloudy ISM (White and Long 1991) model was applied as a more accurate representation, with results given in Table 3 of Leahy et al. (2020). The subset of SNRs with measurements of both forward shock and reverse shock (R_{fs}, EM_{fs}, T_{fs}, EM_{rs} and T_{rs}) were modelled in more detail. We note that R_{rs} is not measured for SNRs. In this case the extra two observed quantities constrain whether the CSM is uniform ($s = 0$) or stellar wind profile ($s = 2$) and distinguish between ejecta profiles (n). 3 of the 12 have $(s, n) = (0,7)$, 4 have (s,n)=(2,7), and 5 have $(s, n) = (2,12)$. Of the 12 SNRs, the 5 Type Ia all have $(s, n) = (2,12)$, i.e. all Type Ia SNRs have occurred in a stellar wind environment.

4. SUMMARY AND CONCLUSION

Supernova remnants (SNRs) play an important role for energy and mass injection into the interstellar medium (ISM). We have developed improved models of SNRs which are readily applied to those SNRs with measured radius, forward shock (fs) emission measure (EM_{fs}) and EM-weighted temperature (T_{fs}) of the fs gas. These models are based on hydrodynamic simulations and cover the stages of evolution including' early ejecta-dominated (ED) phase, the non-radiative ISM dominated phase, and the long transition between the two. The forward shock radius, EM_{fs} and T_{fs} for forward-

shocked (shocked ISM) gas, and EM_{rs} and T_{rs} for reverse-shocked (rs) gas (shocked ejecta) are calculated for the full evolution.

The model allows a wide range of input parameters relevant to SN explosions. These are SN energy, ejected mass, elemental abundances of the ejecta, ejecta envelope power-law index (n), ISM power-law index (s), ISM temperature, ISM abundances, ISM turbulence velocity, and SNR age. Electron heating by Coulomb collisions is automatically included, but T_e/T_{ion} can also be specified by hand. A simple prescription is used to determine when radiative losses set in (following Cioffi et al. 1988). The subsequent radiative phases are calculated according to the prescriptions in Cioffi et al. (1988), with the difference that we smoothly join the start of the radiative evolution onto the end of the adiabatic evolution by matching appropriate boundary conditions.

With the new models, we have studied 3 samples of SNRs. These are 50 SNRs in the LMC with X-ray observations (Leahy, 2017), 15 SNRs in the inner Galaxy with X-ray observations and distance determinations (Leahy & Ranasinghe 2018), and the available set at all Galactic longitudes (excluding the inner Galaxy set of Leahy & Ranasinghe 2018) of 43 Galactic SNRs with distances and X-ray observationis (Leahy et al. 2020). The results of all three analyses are compatible, although the accuracy of the SNR models has been improved between the first study (using the Leahy & Williams 2017 version) and the latest study (using the Leahy et al. 2019 version).

Generally, the explosion energy distribution follows a log-normal distribution, with mean energy $\sim 5 \times 10^{50}$ erg, and the ISM density distribution follows a log-normal distribution, with mean density depending on the SNR sample (highest for the inner Galaxy SNR sample, similar for the LMC and larger Galaxy samples). For the whole Galaxy sample (43 SNRs from Leahy et al. 2020 plus 15 SNRs from Leahy & Ranasinghe 2018) we derive a birthrate, corrected for incompleteness, of $\sim 1/35$yr, which is consistent with the Galactic SN rate (Tammann et al. 1994). Future work will expand the samples which are modelled and further improve the SNR models.

Acknowledgement

References

Bandiera, R.: 2001, 225 *Frontier Objects in Astrophysics and Particle Physics, eds. F. Giovannelli & G. Mannocchi*, 225.

Cioffi, D. F., McKee, C. F., Bertschinger, E.: 1988, *The Astrophysical Journal*, **334**, 252.

Cox, D. P.: 2005, *Annual Reviews of Astronomy & Astrophysics*, **43**, 337.

Leahy, D. A.: 2017, *The Astrophysical Journal*, **837**, 36.

Leahy, D. A., Williams, J. E.: 2017, *The Astronomical Journal*, **153**, 239.

Leahy, D.A., Ranasinghe, S.: 2018, *The Astrophysical Journal*, **866**, 9.

Leahy, D., Wang, Y., Lawton, B. et al.: 2019, *The Astronomical Journal*, **158**, 149.

Leahy, D. A., Ranasinghe, S., Gelowitz, M.: 2020, *The Astrophysical Journal Supplement*, **248**, 16.

Maggi, P., Haberl, F., Kavanagh, P. J. et al.: 2016, *Astronomy & Astrophysics*, 585, A162.

Raymond, J. C., Cox, D. P., Smith, B. W.: 1976, *The Astrophysical Journal*, **204**, 290.

Tammann, G. A., Loeffler, W., Schroeder, A.: 1994, *The Astrophysical Journal Supplement*, **92**, 487.

Truelove, J. K., McKee, C. F.: 1999, *The Astrophysical Journal Supplement*, **120**, 299.

White, R. L., Long, K. S.: 1991, *The Astrophysical Journal*, **373**, 543.